

Macromolecular Materials and Engineering

3D-Printing of High- κ Thiol-Ene Resins with Spiro-Orthoesters as Anti-Shrinkage Additive

--Manuscript Draft--

Manuscript Number:	name.201900515R1
Full Title:	3D-Printing of High- κ Thiol-Ene Resins with Spiro-Orthoesters as Anti-Shrinkage Additive
Article Type:	Full Paper
Section/Category:	
Keywords:	high- κ dielectrics; photopolymerization; thiol-ene click reaction; spiro-orthoesters; anti-shrinkage additives
Corresponding Author:	Frank Wiesbrock, Dr. Polymer Competence Center Leoben Leoben, AUSTRIA
Corresponding Author Secondary Information:	
Corresponding Author's Institution:	Polymer Competence Center Leoben
Corresponding Author's Secondary Institution:	
First Author:	Philipp Marx
First Author Secondary Information:	
Order of Authors:	Philipp Marx
	Angelo Romano
	Ignazio Roppolo
	Angela Chemelli
	Inge Mühlbacher
	Wolfgang Kern
	Sunny Chaudhary
	Thomas Andritsch
	Marco Sangermano
Order of Authors Secondary Information:	Frank Wiesbrock, Dr.
Abstract:	Tri(ethylene glycol) divinyl ether and the spiro-orthoester 2-((allyloxy)methyl)-1,4,6-trioxospiro[4.4]nonane can be formulated in different ratios and crosslinked by thiol-ene reactions. The spiro-orthoester is used as anti-shrinkage additive, enabling shrinkage reduction of up to 39%. Addition of a radical photoinitiator for the thiol-ene reaction and a cationic photoinitiator for the double ring-opening of the spiro-orthoester enables for dual-curing for application in 3D-printing. The formulation free of the spiro-orthoester shows gelation during the printing process and, correspondingly, low resolution. The formulations containing the spiro-orthoester exhibit higher resolutions in the range of 50 μm . The resins containing mixtures of tri(ethylene glycol) divinyl ether and the spiro-orthoester show permittivities as high as 104. The dielectric loss factor of the resins is in the range of 0.5 to 7.6, and the conductivity in the range of $1.3 \cdot 10^{-11}$ to $2.0 \cdot 10^{-11}$ $\text{S} \cdot \text{cm}^{-1}$. These high- κ materials can be 3D-printed by digital light processing for the next generation electronic materials.
Additional Information:	

Question	Response
<p>Please submit a plain text version of your cover letter here.</p>	<p>Dear ladies and gentlemen,</p> <p>On behalf of all co-authors and myself it is my big pleasure to submit the revised version of the manuscript '3D-Printing of High-k Thiol-Ene Resins with Spiro-Orthoesters as Anti-Shrinkage Additive' with the kind request for consideration as a publication in the journal 'Macromolecular Materials and Engineering'.</p> <p>This manuscript describes the crosslinking of tri(ethylene glycol) divinyl ether and the spiro-orthoester 2-((allyloxy)methy)-1,4,6-trioxospiro[4.4]nonane, the latter as anti-shrinkage additive, by thiol-ene reactions. Dual-curing comprising the radical-induced thiol-ene reaction and the cationic ring-opening of the spiro-orthoester was used in 3D-printing. Only the formulations containing both, the tri(ethylene glycol) divinyl ether and the spiro-orthoester exhibited high resolutions in the range of 50 micrometers. Notably, these resins showed permittivities as high as 10'000, qualifying these high-k materials that can be 3D-printed by digital light processing as the next generation of electronic materials.</p> <p>All comments and valuable suggestions for improvements by the reviewers have been considered to fullest extent during the revision of this manuscript and I hope the revised manuscript can be accepted for publication in 'Macromolecular Materials and Engineering'.</p> <p>I look forward to hearing from you and send my best wishes, Frank Wiesbrock</p>
<p>Do you or any of your co-authors have a conflict of interest to declare?</p>	<p>No. The authors declare no conflict of interest.</p>

3D-Printing of High- κ Thiol-Ene Resins with Spiro-Orthoesters as Anti-Shrinkage Additive

Philipp Marx[†], Angelo Romano[†], Ignazio Roppolo, Angela Chemelli, Inge Mühlbacher, Wolfgang Kern, Sunny Chaudhary, Thomas Andritsch, Marco Sangermano, Frank Wiesbrock**

P. Marx, Dr. I. Mühlbacher, Dr. F. Wiesbrock
Polymer Competence Center Leoben GmbH, Roseggerstrasse 12, 8700 Leoben, Austria.
E-mail: frank.wiesbrock@pccl.at

P. Marx, Prof. W. Kern
Chair of Chemistry of Polymeric Materials, Montanuniversitaet Leoben, Otto-Glöckel-Strasse 2, 8700 Leoben, Austria.

A. Romano, Dr. I. Roppolo, Prof. M. Sangermano
Department of Applied Science and Technology, Politecnico di Torino, Corso Duca degli Abruzzi 24, 10129 Torino, Italy.
E-mail: marco.sangermano@polito.it

Dr. A. Chemelli
Institute of Inorganic Chemistry, Graz University of Technology, NAWI Graz, Stremayrgasse 9, 8010 Graz, Austria.

S. Chaudhary, Dr. T. Andritsch
Faculty of Engineering and Physical Sciences, Department of Electronics and Computer Science, University of Southampton, SO17 1BJ Southampton, United Kingdom.

[†] These authors contributed equally to this work and share the first authorship.

Abstract. Tri(ethylene glycol) divinyl ether and the spiro-orthoester 2-((allyloxy)methyl)-1,4,6-trioxospiro[4.4]nonane can be formulated in different ratios and crosslinked by thiol-ene reactions. The spiro-orthoester is used as anti-shrinkage additive, enabling shrinkage reduction of up to 39%. Addition of a radical photoinitiator for the thiol-ene reaction and a cationic photoinitiator for the double ring-opening of the spiro-orthoester enables for dual-curing for application in 3D-printing. The formulation free of the spiro-orthoester shows gelation during the printing process and, correspondingly, low resolution. The formulations

containing the spiro-orthoester exhibit higher resolutions in the range of 50 μm . The resins containing mixtures of tri(ethylene glycol) divinyl ether and the spiro-orthoester show permittivities as high as 10^4 . The dielectric loss factor of the resins is in the range of 0.5 to 7.6, and the conductivity in the range of $1.3 \cdot 10^{-11}$ to $2.0 \cdot 10^{-11} \text{ S} \cdot \text{cm}^{-1}$. These high- κ materials can be 3D-printed by digital light processing for the next generation electronic materials.

Keywords: high- κ dielectrics, photopolymerization, thiol-ene click reaction, spiro-orthoesters, anti-shrinkage additives

1. Introduction

Materials with a permittivity higher than SiO_2 ($\epsilon_r = 3.9$) or even Si_3N_4 ($\epsilon_r = 7$)^[1] are referred to as high- κ dielectrics, which are required for the production of semiconductors.^[2-3] Due to the on-going trend of miniaturization, which still follows the prediction of a doubled number of transistors every two years according to Moore's law,^[4] such materials are in the focus of research and development. As a consequence of the continuous demand for smaller and more complex geometries in the production of integrated circuits, also the processing routines of such high- κ dielectrics need to be addressed, for which photolithographic processes^[5,7] are favorable due to their high spatial resolution.

Since its introduction in the 1980s, 3D-printing has gained attention due to inherent advantages such as the possibility to produce customized parts with complex shapes without the need for molds, low raw material consumption as well as 'production on demand'. Hence, 3D-printing is used in the production processes of numerous industrial sectors such as aerospace and automotive,^[8] biomedicine,^[9] as well as electronics,^[10] in particular for the rapid fabrication of prototypes and final products at low volume. Liquid photopolymers can be 3D-printed by digital light processing DLP, a special type of stereo-lithography. By this

technique, photosensitive resins are cured upon light irradiation. In a DLP printer, a height-adjustable platform is suspended in the resin formulation and illuminated; the targeted specimen is built up layer-by-layer by the z-movement of the platform. Major advantages of the DLP technique are high accuracy and resolution as well as the production of smooth surfaces.

The DLP printability of different monomer classes such as acrylates and methacrylates,^[11] thiol-ene systems,^[12] epoxides,^[13] vinyl ethers,^[14] and hybrid systems^[15] has been investigated. However, acrylates and methacrylates are the most commonly employed for DLP, due to their high reaction rate and their good mechanical properties.^[16] The major drawback of these materials is the volume shrinkage during the curing reaction.^[17] This shrinkage results in the formation of mechanical stresses in the polymer networks,^[18] unfavorably combined with reduced CAD fidelity.

The shrinkage during the curing reaction is caused by the formation of covalent bonds, which are shorter than the van-der-Waals radii between the unreacted monomers.^[19] In order to reduce the polymerization shrinkage, several attempts have been made. The addition of high filler amounts reduces the shrinkage and the formation of micro voids.^[20] However, due to high light absorption coefficients of the fillers and light scattering,^[21] this strategy is limited for the application in DLP. Another approach is the use of hybrid systems based on methacrylates and monomers that show reduced shrinkage such as epoxides.^[15] The best-suited method is the application of expanding monomers such as spiro-orthocarbonates SOCs, spiro-orthoesters SOEs, and bicyclic orthoesters BOEs. These bicyclic monomers polymerize in cationic fashion by double ring-opening and reveal volumetric expansion;^[22] for example, they have been applied as shrinkage-reducing additive for epoxy resins.^[23]

In a previous study we reported the use of SOEs as volume-controlling additive in photocurable thiol-ene reactions.^[24] The thiol-ene click reaction has numerous advantages

such as uniform network formation, high conversions and insensitivity towards water and oxygen,^[25] and thus, a broad range of applications exists for thiol-ene-cured polymers such as polymer synthesis and surface modification,^[26] photolithography^[7] or the preparation of hydrogels.^[27,28] This study, correspondingly, aimed at the 3D-printing of low- or no-shrinkage high- κ polymers. For this purpose, a thiol-ene resin based on pentaerythritol tetrakis(3-mecaptopropionate) 4SH and tri(ethylene glycol) divinyl ether DVE was investigated, the latter of which contains oligo(ethylene glycol) units that are known for their high permittivity.^[29-31] Different amounts of the SOE 2-((allyloxy)methy)-1,4,6-trioxospiro[4.4]nonane were added as anti-shrinkage additive. In order to achieve sufficiently high reaction rates for the printing process, the curing kinetics of the radical-induced thiol-ene network formation and the cationic double ring-opening reaction of the SOE were investigated. Hence, the ratios of the radical and the cationic initiator as well as the sensitizer were carefully adjusted in order to perform both reactions with similar reaction rates. In addition, the mechanical and the dielectric properties of the cured networks were studied in detail aiming to provide a first evaluation of these materials as high- κ dielectrics.

2. Experimental Part

2.1. Materials

DVE, methyl red, phenylbis(2,4,6-trimethylbenzoyl) phosphine oxide BAPO, 2-isopropylthioxathone ITX, γ -butyrolacone, and allyl glycidylether were purchased from Sigma Aldrich. 4SH was obtained from Bruno Bock Chemische Fabrik GmbH & Co. KG. $[(R)\phi_2I]^+[SbF_6]^-$ was purchased from ABCR. All chemicals were used as received without purification. SOE was synthesized from γ -butyrolactone and allyl glycidylether according to a literature procedure.^[24]

2.2. Preparation of the Formulations

The photo-curable formulations were prepared by mixing DVE, 4SH, and SOE in stoichiometric amounts. SOE was added with amounts ranging from 0 to 50 wt% (Table 1).

The initiators BAPO and $[(R)\phi_2I]^+[SbF_6]^-$ as well as the sensitizer ITX were dissolved in the resin by sonication for 30 min at room temperature. BAPO, $[(R)\phi_2I]^+[SbF_6]^-$ and ITX were added in the ratio 0.2:0:0 wt% in the pure resin, and 0.4:1:1 wt% in the formulations containing SOE, respectively. To all formulations, 0.05 wt% of methyl red were added.

FT-IR (ATR, cured resins): ν (cm^{-1}) = 3477, 2866, 1733, 1470, 1414, 1389, 1350, 1288, 1237, 1131, 1098, 1036, 935, 885, 850.

2.3. 3D-Printing of the Formulations

Digital models were 3D-printed using a Freeform Pico Plus 39 DLP printer (Asiga), equipped with a LED light source (405 nm, $8 \text{ mW}\cdot\text{cm}^{-2}$). The nominal XY pixel resolution is 39 μm . The layer thickness was set at 35 μm , and the layer exposure time was 8 sec. After printing, the structures were rinsed with ethanol for 30 sec in order to remove residual non-cured materials. A subsequent post curing process was performed with a medium pressure mercury lamp for 2 min.

2.4. Characterization of the Formulations and the Cured Samples

2.4.1. Determination of the Volumetric Shrinkage

The shrinkage in the course of the curing reaction was quantified gravimetrically by measuring the density of the system before and after curing. The sample used for the shrinkage analyses were prepared by a 3D-printing procedure using a cube structure; the density of the uncured solution was previously measured by weighing a precise amount of the liquid formulation. The shrinkage was calculated according to **Equation 1**.

$$\Delta V(\%) = \frac{\delta_{\text{polymer}} - \delta_{\text{monomer}}}{\delta_{\text{polymer}}} \cdot 100 \quad (\text{Equation 1})$$

2.4.2. FT-IR Measurements

The FT-IR spectra were recorded on a Nicolet iS50 FT-IR spectrometer (Thermo Scientific, Milano, IT) in transmission mode in the range between 450 and 4000 cm^{-1} . In order to monitor the curing kinetic the liquid formulations were placed on a silicon wafer and light-cured with an intensity of 4 $\text{mW} \cdot \text{cm}^{-2}$ under ambient conditions at room temperature. All the samples were cured using a Hamamatsu LC8 lamp with visible bulb and a cut-off filter below 400 nm.

2.4.3 Thermomechanical Properties

DMA measurements were carried out using a Triton Technology TTDMA in the range between -80 and 50 $^{\circ}\text{C}$ at a frequency of 1 Hz and a displacement of 20 μm in order to measure the mechanical properties. The DMA samples were obtained from 3D-printed specimens with a defined thickness of approx. 0.5 mm. DSC measurements were performed with a Netzsch DSC 204 F1 (Netzsch GmbH, Selb, Germany). The samples were heated twice from -65 to 30 $^{\circ}\text{C}$ with a heating rate of 10 $\text{K} \cdot \text{min}^{-1}$. For the determination of the T_g , the second heating cycle was used. The samples were obtained from 3D-printed specimens. For nano-indentation, the samples were measured at room temperature with a Bioindenter TTX-BioUNHT from Anton Paar GmbH, equipped with a ruby-ball tip with a diameter of 200 μm . The maximum load for the indentation experiments was set to values that the penetration depth was approx. 10 μm . The force was increased linearly for 30 sec, held for 30 sec, and finally released for 30 sec. E^* and E_{IT} were determined by fitting the unloading profile according to Oliver & Pharr.^[32]

2.4.4. Dielectric and Electric Properties

The permittivity measurements were performed with a SPECTANO 100 from OMICRON Lab. The samples had a diameter of 80 mm and a height of 0.2 mm and were cured with an intensity of $4 \text{ mW}\cdot\text{cm}^{-2}$ using a Hamamatsu LC8 lamp with visible bulb and a cut-off filter below 400 nm. All samples were thoroughly dried at 80°C in vacuum for 72 h before the measurement. The samples were characterized in a frequency range of 0.1 Hz to 5 kHz at room temperature. For confirmation, the sample SOE 30 was measured with the Solartron of Solartron Analytical, which reproduced the results previously obtained by measurements with the Spectano 100. The DC conductivity measurements were performed by 6517B Electro High Resistance Meter based on the ASTM standard D257–14. The samples were cured with an intensity of $4 \text{ mW}\cdot\text{cm}^{-2}$ using a Hamamatsu LC8 lamp with visible bulb and a cut-off filter below 400 nm. Voltage was applied across the sample for a defined duration: In the present work, the samples were subjected to $500\pm 5\text{V}$ for 1 min according to recommendations of the aforementioned standard. The volume resistivity was calculated according to the equation 2,

$$\rho = \frac{AV}{It_c} \quad (\text{Equation 2})$$

in which ρ is the volume resistivity of the sample, V is the applied voltage, t_c is the thickness of the sample, I is the current reading from the electrometer, and A is the area of the electrode of the test cell (22.9 cm^2 for the tested specimens). The DC conductivity is the inverse of resistivity.

2.4.5. Surface Characterization

The contact angle measurements were performed on a Kruss DSA 100 automated goniometer, using the sessile drop method with distilled water, ethylene glycol, and diiodomethane as test liquids. The surface energy was calculated according to the Owens-Wendt-Rabel-Kaelble (OWRK) method. The zeta potential measurements were conducted on a SurPASS Electrokinetic Analyzer from Anton Paar using a clamping cell. The electrolyte solution was

0.01 M KNO₃ solution. For titration, a 0.05 M HNO₃ solution was used. The 3D-printing experiments were performed on a Pico Plus 39 from Asiga, with x-y-resolution of 39 μm and a light intensity of 8 mW·cm⁻². The layer thickness was 35 μm, and the irradiation time was 8 sec.

3. Results and Discussion

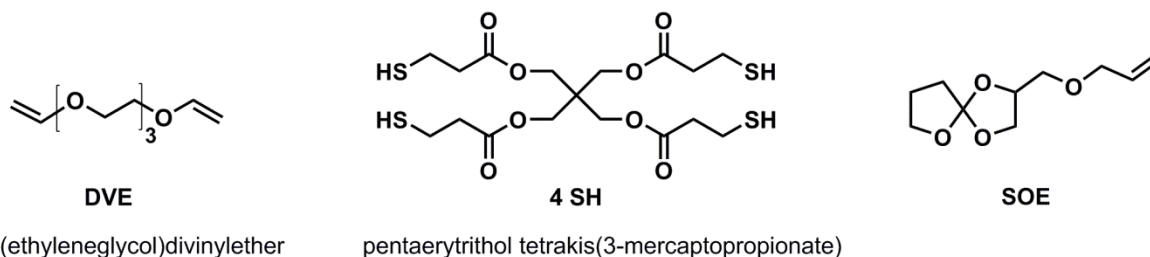
3.1. Preparation of the Formulations and Shrinkage/Expansion Measurements

For the preparation of the photocurable thiol-ene formulations, DVE and 4SH were mixed in stoichiometric amounts (**Figure 1a**). In order to reduce the shrinkage of the system during the crosslinking reaction, the SOE was added with amounts of 10, 20, 30, 40 and 50 wt%, replacing the corresponding amount of DVE (**Table 1**). The SOE was synthesized in a one-step reaction from γ-butyrolactone and allylglycidyl ether according to a precedent study.^[24] The allyl group of the SOE enables the incorporation into the polymer network by the radical-mediated thiol-ene reaction, while the bicyclic SOE unit polymerizes by cationic double-ring opening in the presence of photo-generated acids (Figure 1b and 1c).

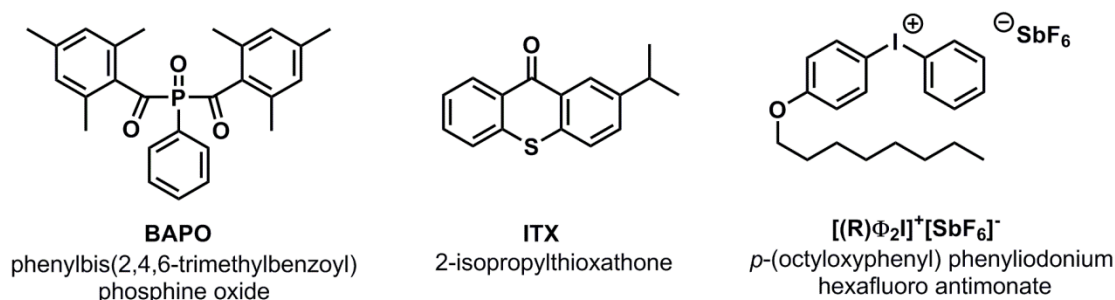
In order to initiate both reactions simultaneously, the radical thiol-ene reaction and the cationic double-ring opening of the SOE, the radical initiator phenylbis(2,4,6-trimethylbenzoyl) phosphine oxide BAPO and the cationic photo-initiator *p*-(octyloxyphenyl) phenyliodonium hexafluoro antimonate [(R)φ₂I]⁺[SbF₆]⁻ as well as the photosensitizer 2-isopropylthioxathone ITX were added to the formulation (Figure 1b and 1c). ITX was added in order to enable the curing reaction at wavelengths above 400 nm by irradiation with visible light. Methyl red was added to all formulations in order to enhance the pot life of the resin and to control the curing depth in the printing process. The volumetric shrinkage upon curing was

calculated from the densities of the resin formulations before and after curing (Equation 1, Table 1).

(a) Chemical structure of the monomers and the crosslinker



(b) Chemical structure of the initiators and the sensitizer



(c) Cationic double ring-opening and radical mediated thiol-ene reaction of the spiroorthoester

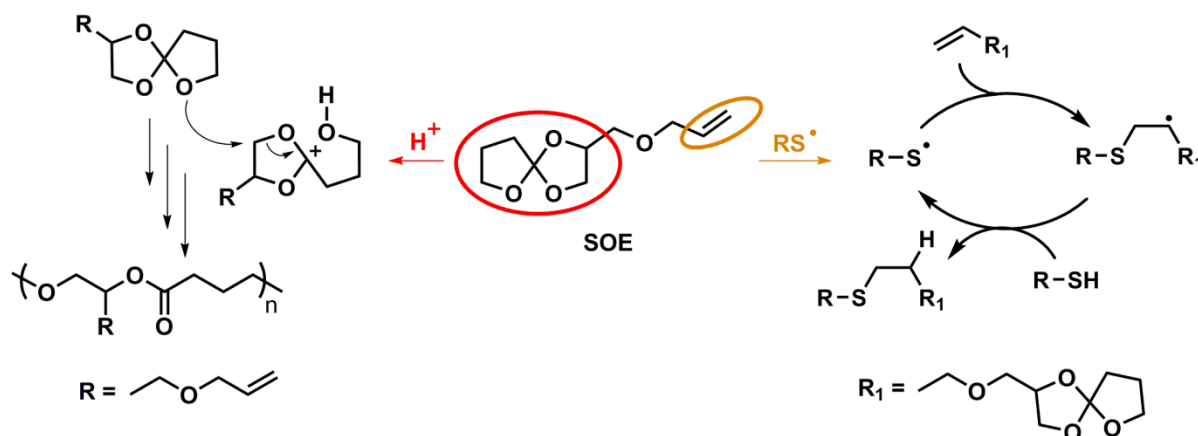


Figure 1. A; top: Chemical structure of the used monomers DVE and SOE and the crosslinker 4SH. B; middle: Chemical structure of the initiators BAPO and $[(R)\Phi_2I]^+[SbF_6]^-$ as well as the sensitizer ITX. C; bottom: Mechanism of the cationic double ring-opening and the thiol-ene reaction of the SOE.

The resin free of the SOE, which was crosslinked by the thiol-ene reaction, exhibited shrinkage of 6.85 vol%. This shrinkage is in the typical range for thiol-ene systems.^[22,23] Upon partial replacement of DVE by the SOE, this shrinkage was reduced due to the double ring-opening of the SOE, during which two covalent bonds are broken upon volumetric expansion.^[22,33] Hence, an increasing amount of SOE results in enhanced reduction of the shrinkage. The formulation containing 50 wt% of the SOE showed the lowest shrinkage of 4.93 vol%, corresponding to an overall shrinkage reduction of 39% compared to the pure SOE-free resin.

Table 1. Composition and volumetric shrinkage all formulations containing thiol-ene resins and SOE.

Formulation	Composition of the formulations			Shrinkage (vol%)
	SOE (wt%)	DVE (wt%)	molar ratio of alkene : thiol groups	
SOE0	0	100	1:1	6.85
SOE10	10	90	1:1	6.81
SOE20	20	80	1:1	6.39
SOE30	30	70	1:1	5.89
SOE40	40	60	1:1	5.57
SOE50	50	50	1:1	4.93

3.2. Monitoring of the Curing Reaction

The network formation occurs upon the radical-mediated thiol-ene click reaction between the double bonds of DVE and the allyl groups of the SOE as well as the thiol groups of 4SH (Figure 1c). The bicyclic SOE group opens according to a cationic double ring-opening mechanism. The kinetics of the light-induced thiol-ene reaction were monitored by the depletion of the signals representing the thiol groups (2569 cm^{-1} , SH stretching vibration) and the carbon double bonds of DVE and SOE (1630 cm^{-1} , C=C stretching vibration) in IR

spectra.¹⁷ Additionally, for the vinylic carbon double bond of DVE the depletion of signals at approx. 960 cm⁻¹ (CH out-of-plane deformation) and 825 cm⁻¹ (CH₂ out-of-plane deformation) was observed. Simultaneously, the curing kinetics of the SOE ring-opening was studied by the depletion of the signal of the SOE group (1050 cm⁻¹). The ring-opening reaction of the SOE is also represented by an increasing signal of the hydroxyl groups in the region between 3100-3700 cm⁻¹.^[17]

The conversion curves (**Figure 2**, right) show the simultaneous occurrence of both, the thiol-ene reaction and the double ring-opening of the SOE in about 60 seconds; the mechanism of the curing reaction, hence, may be referred to as a dual-cure mechanism. The comparison of the conversion curves of formulations without and with SOE reveals that the addition of SOE does not change the reactivity of the thiol-ene reaction, which proceeds with a high reaction rate, due to which a plateau is reached within less than 15 sec (conversion of 94%). Furthermore, the similar conversion of the thiol groups and the carbon double bonds shows that neither homopolymerization of DVE nor secondary reactions occur.

The curing of the SOE reveals two different reactivity regions upon network formation, one from 0 to approx. 15 sec and another one between 30 and 60 sec. These different reactivities are assumed to originate from the gelation of the resin formulation during the polymerization. In the first stage, prior to the gelation of the thiol-ene network, the ring-opening reaction occurs in cationic fashion according to the mechanism described hereinabove (Figure 1c). The reaction of the SOE according to that mechanism can be confirmed by the shifting of the ester signal (from 1725 to 1735 cm⁻¹).^[17] After reaching the gelation point, the lower mobility of the SOE slows down the reaction.

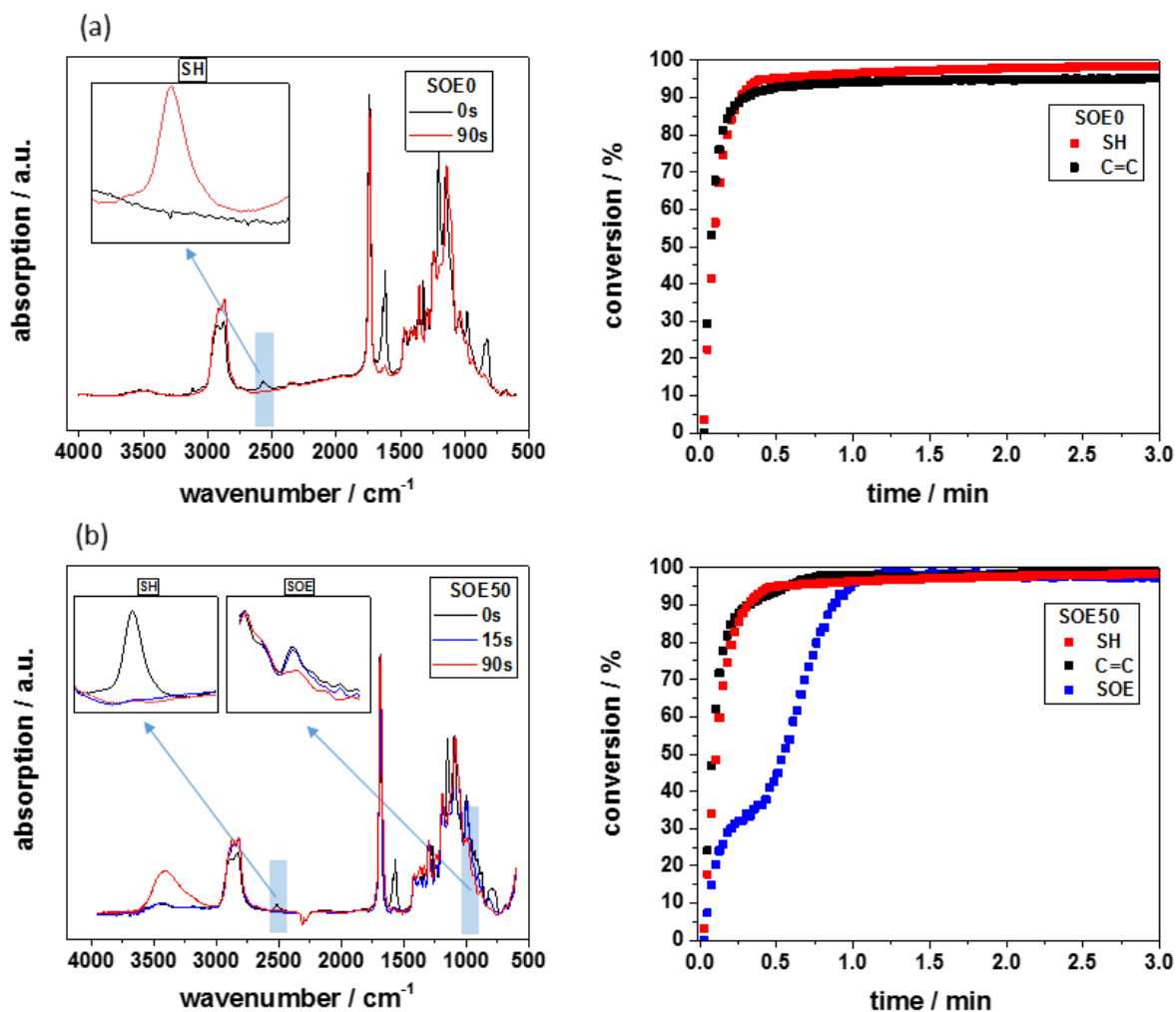


Figure 2. A; top: FT-IR spectrum of the curing of the SOE-free thiol-ene resin (left) and conversion of the C=C double bonds and SH groups (right). B; bottom: FT-IR spectrum of the curing reaction of the formulation containing 50 wt% of SOE (left) and conversion of the C=C double bonds, the SH groups and the SOE groups (right).

Hydroxyl groups (signal at $3100\text{--}3700\text{ cm}^{-1}$) were formed after approx. 15 sec of irradiation. While the formation of the hydroxyl groups is in accordance with the proposed reaction mechanism, its delay of 15 sec might originate from the termination of the ring-opening reaction by proton abstraction after the gelation point. The non-occurrence of hydroxyl group formation in the first reaction step (0-15 sec) can be explained by the higher mobility of the SOEs in this first phase, due to which the termination of the ring-opening polymerization of

the SOE units only takes place to minor extent. In the second step, on the other hand, the lower mobility enables proton abstractions, resulting in the formation of hydroxyl groups.

3.3. Thermomechanical Characterization

In order to characterize the thermomechanical properties of the cured polymer networks, dynamic-mechanical analysis DMA, differential scanning calorimetry DSC, and nano-indentation measurements were performed. DMA measurements (**Figure 3**, top; **Table 2**) revealed that the $\tan \delta$ curves were indicative of the formation of a homogeneous polymer network with a single phase-transition. The data demonstrate that the presence of SOE does not significantly alter the storage modulus of the cured resins. Minor alterations of the glass-transition temperature T_g based on DMA measurements (as well as DSC measurements; see hereinafter), however, could be observed: Samples with SOE contents of 0 and 10 wt% showed the same T_g of $-30\text{ }^{\circ}\text{C}$; for SOE contents higher than 10 wt%, a slight decrease of the T_g value was observed with the lowest value of $-35\text{ }^{\circ}\text{C}$ for the SOE50 sample. The trend of decreasing T_g with increasing SOE contents was confirmed by DSC analyses that revealed T_g values in the range from -33 to $-40\text{ }^{\circ}\text{C}$ (**Figure 3**, bottom; **Table 2**).

Concomitant with an increasing SOE content, a slight increase of the $\tan \delta$ value and a slight increase of the full width at half maximum fwhm were observed in the DMA measurements. According to literature,^[34] $\tan \delta$ correlates with the polymer network density and fwhm correlates to the homogeneity of the polymer network. Correspondingly, the addition of SOE slightly decreases the network density and homogeneity (**Table 2**). This effect becomes more pronounced with increasing SOE content, and it could be related to the fact that SOE is a monofunctional allyl ether, while DVE is a bifunctional vinyl ether. In fact, a decrease of the storage modulus in the rubbery plateau by increasing the SOE content was observed (**Figure 3a**). This is consistent with a decrease of cross-linking density.^[35]

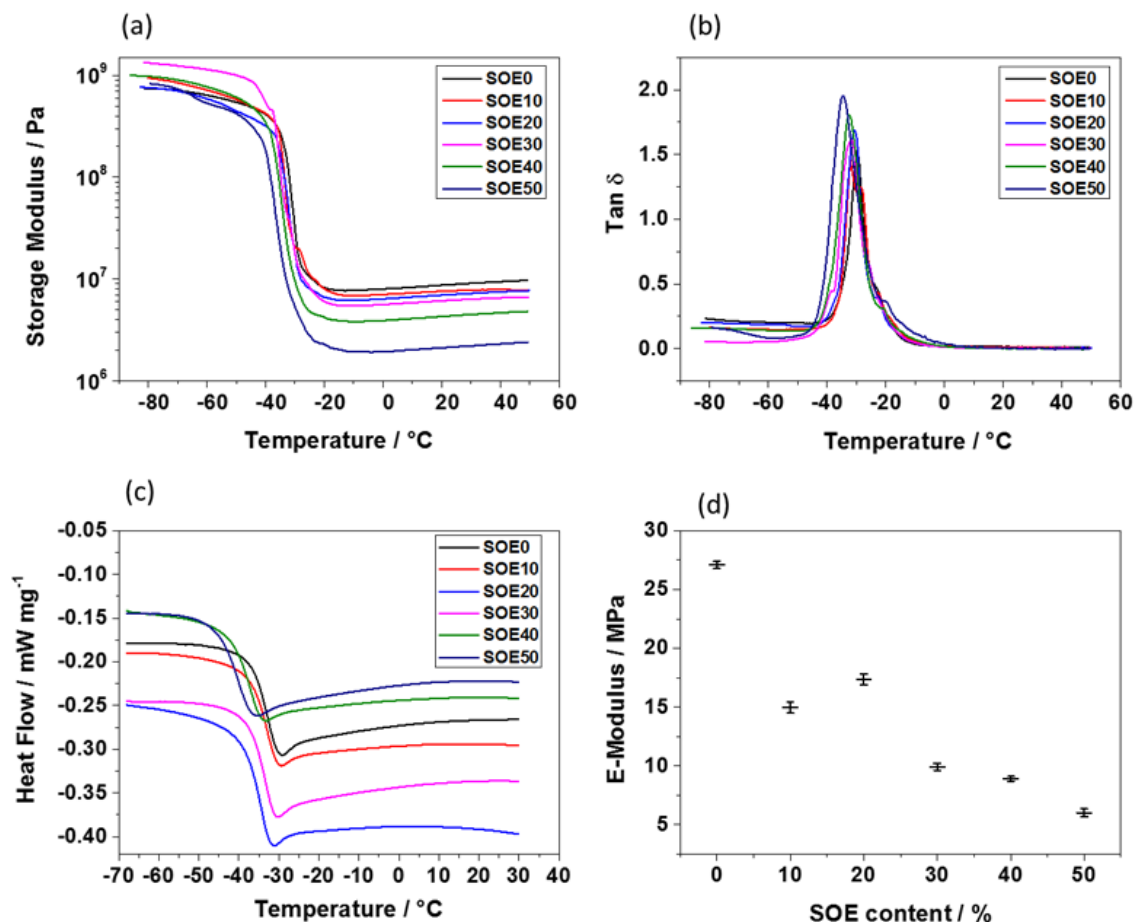


Figure 3. A; top left: Storage modulus of the crosslinked polymers according to DMA measurements. B; top right: Tan δ values of the crosslinked polymers according to DMA measurements. C; bottom left: T_g values of the crosslinked polymers according to DSC measurements. D; bottom right: E-modulus of the crosslinked polymers determined by nanoindentation.

The E-modulus of the polymer networks was determined by nano-indentation measurements (the error bars show two standard deviations, which correspond to a confidence interval of 95%); it was found to decrease upon the addition of SOE (Figure 3d). The decreasing stiffness is in good agreement with results from DMA and DSC measurements that revealed a decrease of the T_g and the network density.

Table 2. T_g values according to DSC and DMA measurements as well as the values of $\tan\delta$ and fwhm according to DMA measurements.

Formulation	DSC	DMA		
	T_g (°C)	T_g (°C)	$\tan\delta$	fwhm
SOE0	−33	−30	1.51	7.2
SOE10	−33	−30	1.44	7.2
SOE20	−35	−31	1.67	7.3
SOE30	−34	−32	1.62	8.5
SOE40	−37	−33	1.80	9.5
SOE50	−40	−35	1.94	11

3.4. Dielectric and Electrical Characterization

The relative permittivity describes the interactions of a medium with electric fields, in particular the polarization and its capability to store charges. If an alternating electric field is applied to a dielectric material, the charge carriers are orientated along the vector of the electric field. Since this polarization does not react instantaneously to the external stimuli, a phase shift between the applied external field and the response of the material occurs. Hence, the permittivity can be described as a complex function containing the real part ϵ' and the imaginary part ϵ'' . While the real part ϵ' describes the ability of a material to store energy, the imaginary ϵ'' part is indicative of the loss of energy.

The relative permittivity of the SOE-free thiol-ene network and the polymer networks containing 10 to 50 wt% SOE were measured at room temperature and frequencies ranging from 0.1 Hz to 5 kHz (**Figure 4a**). The real part of the permittivity of the SOE-free network, hence the network with the highest content of oligo(ethylene glycol) units, increases from approx. 6 to 100 with decreasing frequency. This high permittivity was referred to the facts that poly(ethylene glycol) PEG chains easily rotate around the C-O bonds and that PEG

networks can be easily polarized. Notably, high values of the permittivity were reported as well for other oligo(ethylene glycol)-containing networks and PEG.^[27-29]

The materials containing 10 to 50 wt% of SOE showed even higher permittivity, in particular at the lower range of frequencies: At frequencies below 40 Hz, the permittivity increases significantly and reaches values as high as 10^4 at 0.1 Hz. These values are in the same range like for PEG-based solid polymer electrolytes,^[36-37] and, at the current state of knowledge, are attributed to charge accumulation at the electrode-polymer interface, which partially blocks the charge transport.^[38] The high permittivity values of the networks containing SOE are indicative of conductivities higher than those of common polymeric insulators (for the conductivity measurements themselves, see hereinafter). Additionally, the negative and (in good approximation) linear slope of the imaginary part of the permittivity over the whole range of frequencies is indicative of a fairly conductive material as well. The real part of the permittivity increases with the amount of SOE. This trend is most pronounced at frequencies below 100 Hz. During the cationic double-ring opening of the SOE groups, highly flexible polyester-*co*-polyether chains are formed, and hence, the flexibility and the polarizability of the material increase. This explanation is also in agreement with the decrease of T_g (Table 2) and the decrease of the E-modulus (Figure 3d) upon the addition of SOE.

The imaginary part ϵ'' of the relative permittivity increases with decreasing frequency (Figure 4b). In the double logarithmic plot, an almost linear correlation between ϵ'' and the frequency can be observed. The materials containing SOE exhibit 10 to 100 times higher ϵ'' values than the SOE-free resin. The increase of the permittivity with increasing amount of SOE, which was observed in the real part and explained herein above, is reproduced in the imaginary part as well.

The loss factor $\tan\delta$ is defined as the ratio of the imaginary part ϵ'' and the real part ϵ' of the relative permittivity. It quantifies the dissipation of electromagnetic energy, e.g. into heat.

While an applicable dielectric would show only minimum losses of energy ($\tan \delta < 10^{-4}$), an ideal conductor would not store any energy ($\tan \delta = \infty$). The loss factor of the SOE-free network exhibits values between 0.02 (5 kHz) and 6.5 (0.1 Hz) and increases with decreasing frequency (Figure 4c). While the SOE-free material shows low loss factors at frequencies above 1 kHz ($\tan \delta < 0.1$), it still may not be considered as a good dielectric in that frequency range: If AC voltage was applied, high thermal losses would occur ($\tan \delta$ is related to heat generated in the insulator as result of said losses).

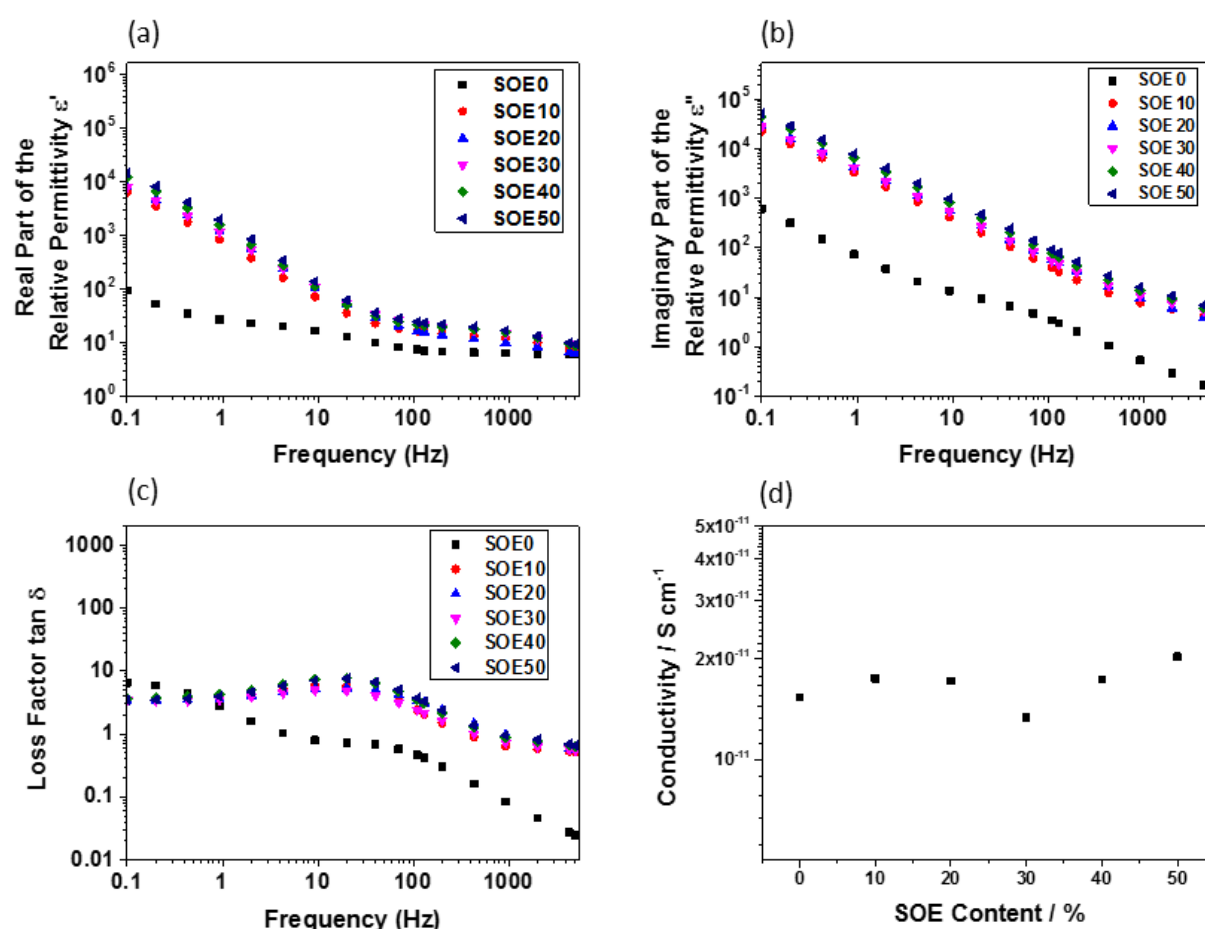


Figure 4. A; top left: Real part of the permittivity ϵ' . B; top right: Imaginary part of the permittivity ϵ'' . C; bottom left: Loss factor $\tan \delta$. D; bottom right: Electrical conductivity of the networks according to the standard ASTM D257.

The dissipation factors of the specimens containing SOE are in the range of 0.5 to 7.6, and are higher than the loss factors of the SOE-free resin, except at low frequencies from 0.1 to 1 Hz. At a frequency of approx. 20 Hz, the loss factor has a local maximum. Since this maximum cannot be observed in the SOE-free resin, the reason is most likely a relaxation process of structural segments related to the double ring-opening of the SOE units, such as the formed polyester-*co*-polyether chains or hydroxyl groups and the correspondingly facilitated absorbance of water (cp. FT-IR spectra in Figure 2, left): In epoxy resins, β -relaxation is observed around 10^4 Hz, which is also related to the presence of hydroxyl groups; the peak for ad- and absorbed water is observed between 1 and 50 Hz.

Since the permittivity measurements revealed a high amount of free charge carriers, the conductivity was measured in order to thoroughly characterize the electrical properties of the materials. These measurements were performed at room temperature according to the standard ASTM D257. The averaged conductivities (Figure 4d) were calculated based on the last ten points of the measurements, after stable current conditions had been reached. All materials show a similar conductivity in the range of $1.3 \cdot 10^{-11}$ to $2.0 \cdot 10^{-11} \text{ S} \cdot \text{cm}^{-1}$. These values are several magnitudes higher than in typically applied insulating polymers ($< 10^{-16} \text{ S} \cdot \text{cm}^{-1}$).

3.5. Surface Polarity

After the completed curing reaction, hydroxyl groups were detected in the polymer networks according to the FT-IR measurements (see hereinabove). Due to their possible impact on the surface polarity of the cured networks, the surface energy and the zeta potential of the materials were determined (**Figure 5**). The surface energy was obtained from contact angle measurements with the three test liquids water, diiodomethane, and ethylene glycol and

calculated according Owens-Wendt-Rabel-Kaelble. All surface energies were in the range of 52 to 60 mN·m⁻¹ and are in good agreement with literature data for thiol-ene resins.^[39] Even for the zeta potential measurements, which are very sensitive towards surface charges, only a slight shift of the isoelectric point IEP from approx. 3.7 to 4.1 was detected for the networks containing 40 and 50% SOE. Hence, the surface energy and zeta potential measurements clearly revealed that there are only negligible changes in surface polarity of the cured networks.

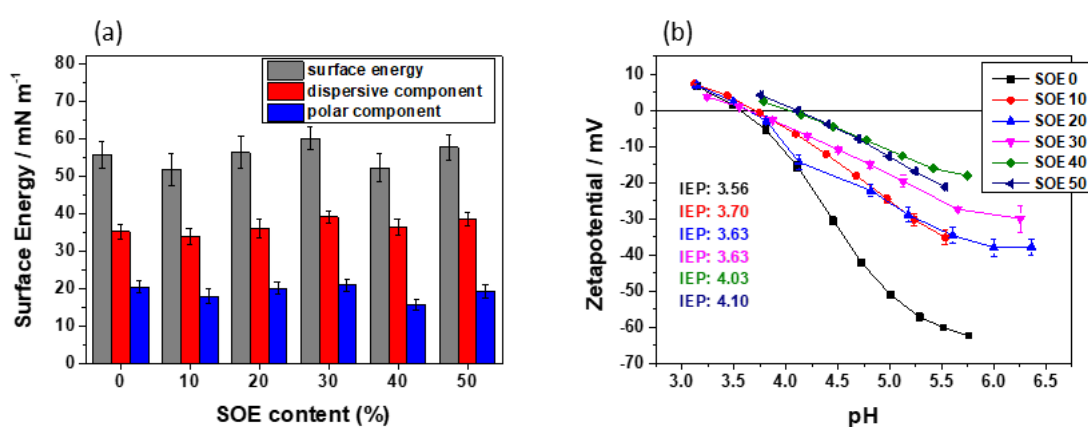


Figure 5. A; left: Surface energies calculated from contact angle measurements. B; right: Zeta potential measurements of the SOE-free resin and the resins containing 0 to 50 wt% SOE.

3.6. 3D-Printing

The thiol-ene resin formulations were finally tested as materials for 3D printing. The printing of the resins was performed with DLP equipment with a light source in the visible region. The SOE-free resin showed rapid gelation upon irradiation in the printing process, resulting in insufficient resolution. The formulations containing SOE, on the other hand, exhibited a pronouncedly better performance than the SOE-free resin. After an optimization of the printing parameters and the addition of 0.05 wt% methyl red in order to control the curing depth and to enhance the pot life of the formulations, high-resolution structures were printed

successfully (**Figure 6a** and **6b**). Different resolution among the SOE-free and the SOE-containing specimens was observed (Figure 6b); this could be related to both a better control of thiol-ene reaction and to the reduced shrinkage due to the addition of SOE. In fact, for the SOE30 specimen, a resolution of 50 μm was obtained (Figure 6c), which was defined based on shape deviations of the printed specimen from the CAD design such as blurring on the edges of the honeycomb structure. The SOE-free formulation, on the other hand, showed a resolution in the range of 100-200 μm . Notably, the resolution of 50 μm is in the range of the nominal XY pixel resolution of 39 μm of the DLP equipment.

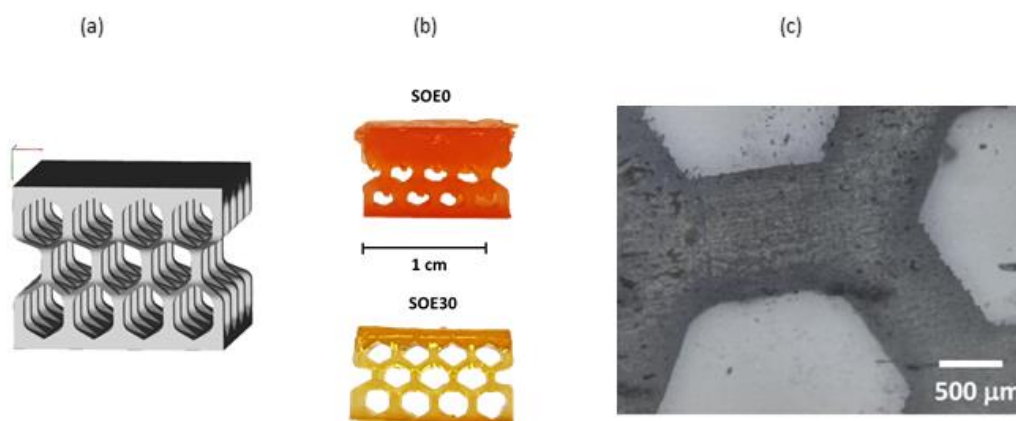


Figure 6. A, left: CAD drawing of the structure to be 3D-printed. B, middle: Photography of the 3D-printed structure of the formulation containing 0 and 30 wt% of SOE (SOE0 and SOE30), respectively. C; right: Light microscopic photography of a section of the specimen SOE30.

4. Conclusion & Outlook

Resin formulations containing the monomers DVE and SOE can be crosslinked according to a dual-cure mechanism, comprising the radical thiol-ene reaction of DVE and SOE with the mercapto compound 4SH as well as the cationic double-ring opening of the SOE. In this study, formulations containing 0, 10, 20, 30, 40, and 50 wt% of SOE were investigated. If, in addition to a radical and a cationic photo-initiator such as BAPO and the iodonium salt

416 $[(R)\phi_2I]^+[SbF_6]^-$, sensitizers such as ITX are used, the dual curing can be triggered by stimuli
 417 such as visible light. If a wt%:wt% = 50:50 mixture of DVE and SOE is used, the shrinkage
 418 during curing can be reduced by 39% in comparison to a SOE-free mixture.

419 The real part of the permittivity of the SOE-free network increased from approx. 6 to 100 with
 420 decreasing frequency, qualifying this material with a high abundance of oligo(ethylene
 421 glycol) units as a high- κ dielectric.. The loss factors of the SOE- containing resins are in the
 422 range of 0.5 to 7.6. At a frequency of approx. 20 Hz, the loss factor has a local maximum,
 423 which was referred to ad- and absorbed water due to the presence of hydroxyl groups in those
 424 resins. Conductivity measurements revealed that all resins show conductivity in the range of
 425 $1.3 \cdot 10^{-11}$ to $2.0 \cdot 10^{-11}$ S·cm⁻¹, which is several magnitudes higher than that of common
 426 polymer systems.

427 The printability of the resins was evaluated in DLP printing, during which the SOE-free resin
 428 showed rapid gelation upon irradiation in the printing process and a resulting low resolution
 429 of up to 200 μ m. Precedent kinetic studies had revealed a two-phase curing of the SOE
 430 (before and after the gelation point) and the abovementioned reduced shrinkage. Hence, the
 431 formulations containing SOE exhibited higher resolutions; for the SOE30 specimen, a
 432 resolution of 50 μ m was observed.

433 Considering the good processability and stability in the printing process as well as the reduced
 434 shrinkage, the DVE/SOE formulations seem to be favorable for 3D printing, in particular
 435 compared to commonly used acrylate-/methacrylate-based systems that show an average
 436 shrinkage of more than 12 vol%. Further studies will address the increased mechanical
 437 stability of SOE-rich resins as well as a decreased dielectric loss; for the realization of both
 438 strategies, nanocomposites based on DVE/SOE resins will be developed.

Conflict of Interest

The authors declare no conflict of interest.

Acknowledgement

The research work was performed within the K-Project 'PolyTherm' at the Polymer Competence Center Leoben GmbH (PCCL, Austria) within the framework of the COMET-program of the Federal Ministry for Transport, Innovation and Technology and the Federal Ministry for Digital and Economic Affairs with contributions by the Polytecnico di Torino, the University of Southampton, the Montanuniversitaet Leoben and the Graz University of Technology (Institute for Chemistry and Technology of Materials and the Somapp Lab, a core facility supported by the Austrian Federal Ministry of Education, Science and Research, the Graz University of Technology, the University of Graz and Anton Paar GmbH). Funding is provided by the Austrian Government and the State Government of Styria.

Literature

- [1] G. D. Wilk, R. M. Wallace, J. M. Anthony, *J. Appl. Phys.* **2001**, 89, 5243.
- [2] R. A. Ortiz, A. Facchetti, T. J. Mars, *Chem. Rev.* **2010**, 110, 205.
- [3] R. Popielarz, C. K. Chiang, R. Nozaki, J. Obrzut, *Macromolecules* **2001**, 34, 5910.
- [4] G. E. Moore, *Electronics* **1965**, 38, 114.
- [5] T. Griesser, J. C. Kuhlmann, M. Wieser, W. Kern, G. Trimmel, *Macromolecules* **2009**, 42, 725.

- [6] M. Fimberger, A. Behrendt, G. Jakopic, F. Stelzer, V. Kumbaraci, F. Wiesbrock, *Macromol. Rapid Commun.* **2016**, 37, 233.
- [7] V. Schenk, L. Ellmaier, E. Rossegger, M. Edler, T. Griesser, G. Weidinger, F. Wiesbrock, *Macromol. Rapid Commun.* **2012**, 33, 396.
- [8] V. Petrovic, J. V. H. Gonzalez, O. J. Ferrando, J. D. Gordillo, J. R. B. Puchades, L. P. Griñan, *Int. J. Prod. Res.* **2011**, 49, 1061.
- [9] S. Stassi, E. Fantino, R. Calmo, A. Chiappone, M. Gillono, D. Scaiola, C. F. Pirri, C. Ricciardi, A. Chiadò, I. Roppolo, *ACS Appl. Mater. Interfaces* **2017**, 9, 19193.
- [10] E. Fantino, A. Chiappone, I. Roppolo, D. Manfredi, R. Bongiovanni, C. F. Pirri, F. Calignano, *Adv. Mater.* **2016**, 28, 3712.
- [11] C. Gorsche, K. Seidler, P. Knaack, P. Dorfinger, T. Koch, J. Stampf, N. Moszner, R. Liska, *Polym. Chem.* **2016**, 7, 2009.
- [12] L. Chen, Q. Wu, G. Wei, R. Liu, Z. Li, *J. Mater. Chem. C* **2018**, 6, 11561.
- [13] A. P. Melisaris, S. D. Hanna, T. H. Pang, (Ciba SpecialtyChemicals Corp.), U.S. Patent 6099787, 2000.
- [14] S. C. Lapin, J. R. Snyder, E. V. Sitzmann, D. K. Barnes, G. D. Green, (AlliedSignal Inc.), U.S. Patent 5437964, 1995.
- [15] S. Lantean, I. Roppolo, M. Sangermano, C. F. Pirri, A. Chiappone, *Inventions* **2018**, 3, 29.
- [16] G. Taormina, C. Sciancalepore, M. Messori, F. Bondioli, *J. Appl. Biomater. Fundam. Mater.* **2018**, 16, 151.
- [17] K. Miyazaki, T. Takata, T. Endo A. Inanaga, *Dent. Mater. J.* **1994**, 13, 9.

- 483 [18] H. Lu, J. W. Stansbury, S. H. Dickens, F. C. Eichmiller, C. N. Bowman, *J. Biomed.*
 484 *Mater. Res. Part B: Appl. Biomater.* **2004**, 71, 206.
- 485 [19] R. F. Brady Jr., *J. Macromol. Sci. Part C* **1992**, 32, 135.
- 486 [20] C. T. W. Meereis, E. A. Münchow, W. L. de Oliveira da Rosa, A. Fernandes da Silva, E.
 487 Piva, *J. Mech. Behav. Biomed. Mater.* **2018**, 82, 268.
- 488 [21] H. Althues, J. Henle, S. Kaskel, *Chem. Soc. Rev.* **2007**, 36, 1454.
- 489 [22] T. Takata, T. Endo, *Prog. Polym. Sci.* **1993**, 18, 839.
- 490 [23] R. A. Ortiz, M. L. B. Duarte, A. G. S. Gómez, M. Sangermano, A. E. G. Valdez, *J.*
 491 *Macromol. Sci. Part A: Pure Appl. Chem.* **2012**, 49, 361.
- 492 [24] P. Marx, A. Romano, R. Fischer, I. Roppolo, M. Sangermano, F. Wiesbrock, *Macromol.*
 493 *Mater. Eng.* **2019**, 4, 1800627.
- 494 [25] M. J. Kade, D. J. Burke, C. J. Hawker, *J. Polym. Sci. Part A: Polym. Chem.* **2010**, 48,
 495 743.
- 496 [26] B. Iskin, G. Yilmaz, Y. Yagci, *Chem. Eur. J.* **2012**, 48, 10254.
- 497 [27] T. R. Dargaville, R. Forster, B. L. Farrugia, K. Kempe, L. Voorhaar, U. S. Schubert, R.
 498 Hoogenboom, *Macromol. Rapid Commun.* **2012**, 33, 1695.
- 499 [28] A. M. Kelly, F. Wiesbrock, *Macromol. Rapid Commun.* **2012**, 33, 1632.
- 500 [29] N. Koizumi, T. Hanai, *Bullet. Inst. Chem. Res.* **1964**, 42, 115.
- 501 [30] R. J. Sengwa, K. Kaur, R. Chaudhary, *Polym. Int.* **2000**, 49, 599.
- 502 [31] S. Mashimo, S. Yagihara, *Macromolecules* **1984**, 17, 630.
- 503 [32] W. C. Oliver, G. M. Pharr, *J. Mat. Res.* **1992**, 7, 1564.

- 504 [33] M. Sangermano, R., A. Ortiz, B. A. Puente Urbina, L. B. Duarte, A. E. G. Valdez, R. G.
1 Santos, *Eur. Polym. J.* **2008**, *44*, 1046.
- 2
3
4
5 506 [34] A. Chiappone, E. Fantino, I. Roppolo, M. Lorusso, D. Manfredi, P. Fino, C. F. Pirri, F.
6
7
8 507 Calignano, *ACS Appl. Mater. Interfaces* **2016**, *8*, 5627.
- 9
10
11 508 [35] A. Chiappone, S. Jeremias, R. Bongiovanni, M. Schonhoff, *J. Polym. Sci. Part B: Polym.*
12
13 509 *Phys.* **2013**, *51*, 1571.
- 14
15
16 510 [36] Y. G. Marinov, G. B. Hadjichristov, A. G. Petrov, H. K. Koduru, L. Marino, N.
17
18
19 511 Scaramuzza, *J. Phys. Conf. Ser.* **2017**, *794*, 012020.
- 20
21
22 512 [37] A. Arya, S. Sharma, A. L. Sharma, D. Kumar, M. Sadiq, *Asian J. Engin. Appl. Technol.*
23
24 513 **2016**, *5*, 4.
- 25
26
27 514 [38] M. Q. A. Al-Gunaid, A. M. N. Saeed, *J. Appl. Polym. Sci.* **2018**, *135*, 45852.
- 28
29
30
31 515 [39] Y. Du, J. Xu, J. D. Sakizadeh, D. G. Weiblen, A. V. Mc Corman, L. F. Francis, *Appl.*
32
33 516 *Mater. Interf.* **2017**, *9*, 24976.

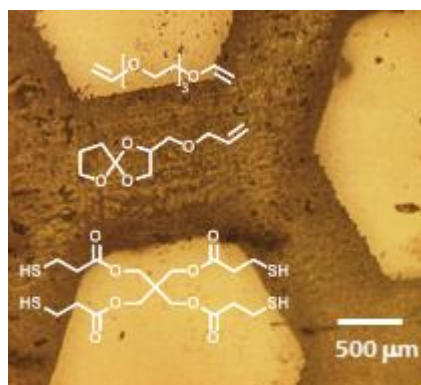
517

TOC Entry

The shrinkage of tri(ethylene glycol) divinyl ether based thiol-ene resins is reduced by 39% using bicyclic spiro-orthoesters as anti-shrinkage additive. A dual-cure mechanism enables 3D-printing of the resin formulations by digital light processing with resolutions in the range of 50 μm . The high permittivity enables potential applications as high- κ material.

P. Marx, A. Romano, I. Roppolo, A. Chemelli, I. Mühlbacher, W. Kern, S. Chaudhary, T. Andritsch, M. Sangermano,* F. Wiesbrock*

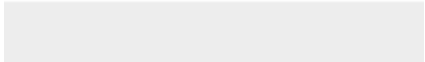

3D-Printing of High- κ Thiol-Ene Resins with Spiro-Orthoesters as Anti-Shrinkage Additive





[Click here to access/download](#)

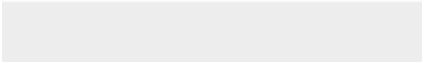

Production Data
Figure01.tif





[Click here to access/download](#)

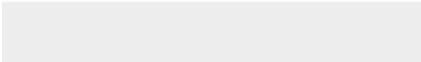

Production Data
Figure02.tif





[Click here to access/download](#)

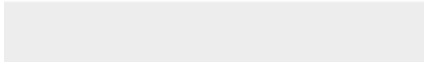
Production Data
Figure03.tif





[Click here to access/download](#)

Production Data
Figure04.tif





[Click here to access/download](#)

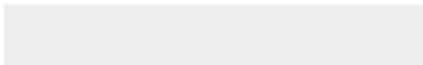
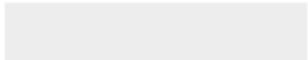
Production Data
Figure05.TIF

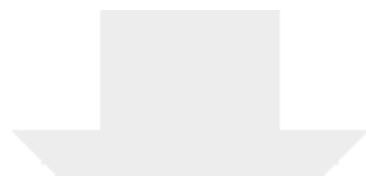




[Click here to access/download](#)

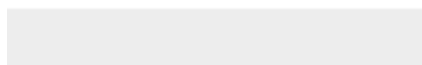
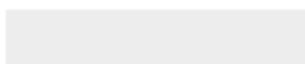
Production Data
Figure06.tif





[Click here to access/download](#)

Production Data
MAME_20190918_PD.docx





Click here to access/download
Production Data
ToC.tif